J. Fluid Mech. (2007), *vol.* 592, *pp.* 471–494.
doi:10.1017/S0022112007008609 Printed in the United Kingdom

Preservation of statistical properties in large-eddy simulation of shear turbulence

P. GUALTIERI[1], C. M. CASCIOLA[1], R. BENZI[2] AND R. PIVA[1]

[1]Dipartimento di Meccanica e Aeronautica, Università di Roma La Sapienza, Via Eudossiana 18, 00184 Roma, Italy

[2]Dipartimento di Fisica e INFM, Università di Roma, Tor Vergata, Via della Ricerca scientifica 1, 00133 Roma, Italy

(Received 12 October 2006 and in revised form 12 August 2007)

We discuss how large-eddy simulation (LES) can be properly employed to predict the statistics of the resolved velocity fluctuations in shear turbulence. To this purpose an *a posteriori* comparison of LES data against filtered direct numerical simulation (DNS) is used to establish the necessary conditions that the filter scale L_F must satisfy to achieve the preservation of the statistical properties of the resolved field. In this context, by exploiting the physical role of the shear scale L_S, the Kármán–Howarth equation allows for the assessment of LES data in terms of scale-by-scale energy production, energy transfer and subgrid energy fluxes. Even higher-order statistical properties of the resolved scales such as the probability density function of longitudinal velocity increments are well reproduced, provided the relative position of the filter scale with respect to the shear scale is properly selected. We consider here the homogeneous shear flow as the simplest non-trivial flow which fully retains the basic mechanism of turbulent kinetic energy production typical of any shear flow, with the advantage that spatial homogeneity implies a well-defined value of the shear scale while numerical difficulties related to resolution requirements in the near wall region are avoided.

1. Introduction

Large-eddy simulation (LES) is a challenging technique for the numerical analysis of turbulent flows in simple and complex geometries (Moin 2002). The idea is to resolve explicitly the non-isotropic and non-homogeneous dynamics of the large scales while accounting for the small scales by a suitable approximation. For reviews see Lesieur & Metais (1996), Meneveau & Katz (2000) and Pope (2000). The original idea was essentially inspired by Kolmogorov view of turbulence (see e.g. Frisch 1995). According to Kolmogorov (1941), the statistical properties of turbulent flows are universal at small scales, regardless of the specific energy forcing mechanism. In this framework, universality means that, for fixed geometry, the statistics of the small-scale fluctuations depend on the Reynolds number Re as the only relevant parameter. In the early attempts, this concept was instrumental in approximating inertial-range effects by defining in a suitable way an eddy viscosity (see e.g. Smagorinsky 1963; Lilly 1967). Despite a number of successive proposals, eddy viscosity is still an important tool for numerical simulations in many applications (see e.g. Moin & Apte 2006).

When viewed rigorously, however, small-scale universality is still an open question. Also, the technique based on $SO(3)$ decomposition has been extensively applied to

show that the isotropic fluctuations dominate the small-scale dynamics (Biferale & Procaccia 2005), although large-scale fluctuations are strongly anisotropic. These results concern the effect of the shear as a small perturbation acting on an otherwise isotropic flow.

However, in most applications, the shear is sufficiently strong to invalidate perturbative approaches. In such conditions, persistence of anisotropy is often observed, either in experiments – for turbulent boundary layers see Saddoughi & Veeravalli (1994); Kurien & Sreenivasan (2002), for free shear flows see Shen & Warhaft (2000); Warhaft & Shen (2002) – or in numerical simulations Spalart (1988); Antonia, Djenidi & Spalart (1994); Pumir & Shraiman (1994). This behaviour is typical of the close proximity of a solid wall as discussed in Pope (2004) and Langford & Moser (1999). See also the discussion reported in Durbin & Speziale (1997). In fact, the interaction between a solid wall and the turbulence results in strongly anisotropic turbulent kinetic energy production which affects most of the turbulent eddies. Hence the range of scales where isotropization might occur is limited. In this context, the concept of the shear scale originally proposed by Corrsin (1958) has been illuminating. The shear scale L_S ideally separates the production-dominated scales from those where inertial transfer takes over. The exact scale-by-scale energy budget was performed in Casciola *et al.* (2003) and Marati, Casciola & Piva (2004) starting from DNS data of a homogeneous shear flow and of a turbulent channel flow, respectively. Successively, the position of the shear scale has been found crucial for small-scale isotropy recovery under intense shear (Casciola *et al.* 2005). As we will see, this kind of reasoning is important for LES where small-scale velocity fluctuations are filtered out at some scale L_F with the overall idea maintaining their dynamical effects on the large scales.

In fact, LES is affected by a systematic error owing to the replacement of the small-scale dynamics with the subgrid model and by a numerical error due to the finite accuracy of the solution of the modelled equations on a grid of size Δ. The sensitivity of the results to these two sources of error has been studied by Klein (2005) and Freitag & Klein (2006) in the context of implicit filtering. The same issue was addressed by Guerts & Frohlich (2002) and Meyers, Guerts & Baelmans (2003) where modelling and numerical errors were parameterized in terms of subgrid activity – ratio of turbulent to total dissipation rate – and subgrid resolution L_F/Δ. Apart from this kind of error which is intrinsic to the methodology, LES calculations depend on the choice of the artificial parameter L_F (see e.g. Baggett, Jimenez & Kravshenko 1997; Jimenez & Moser 2000; and Pope 2004). Here, we attempt to assess the role of the coarse-graining scale L_F in a flow with a given shear scale L_S. Concerning the subgrid model, we adopt deconvolution methods which have received a great deal of attention lately (Stolz & Adams 1999; Stolz, Adams & Kleiser 2001). See also Guerts (1997) Domaradsky & Saiki (1997), Domaraksy & Loh (1999) and Guerts & Holm (2003) for other related approaches, or the contributions by Mathew *et al.* (2003, 2006) which propose to evolve the deconvolved field directly. In deconvolution methods, the *ADM* (Stolz & Adams 1999) in our case, the essential part of the subgrid stress, the so-called resolved stresses (Carati, Winckelmans & Jeanmart 2001), is estimated by reconstructing the fine-grained field via an approximate inversion of the filtering operator whereas the contributions of the unresolved stresses are modelled via a purely dissipative term, i.e. the relaxation term.

We consider here the simplest case of anisotropic turbulence, namely the homogeneous shear flow in a confined box. This flow is a bridge between the strongly idealized homogeneous isotropic turbulence and the more realistic shear flows such

as wall-bounded flows. Actually, the production of turbulent kinetic energy is fully retained, so that the effect of changing the filter scale L_F can be discussed in a much cleaner form. In principle, the filter may directly affect the production range for $L_F > L_S$, or it may influence only the transfer dominated range when $L_F < L_S$. In any case, because of spatial homogeneity, the shear scale is fixed and additional difficulties introduced by the presence of the wall, for example, spatial energy fluxes, are avoided. Moreover, in the homogeneous shear flow, the mean velocity profile in imposed, hence the effect of any LES model on the statistical properties of the velocity fluctuations can be analysed more easily since the production term is affected only by the calculated turbulent fluctuations. On the other hand, for wall-bounded flows, both the fluctuations and the mean flow contribute to the value of the production term.

From the above discussion we argue that LES might preserve the statistical properties of the resolved fluctuations as far as $L_F < L_S$. This is the main question addressed in the paper. We propose here to employ the Kármán–Howarth budget to establish whether the dynamics of the resolved field is altered by the LES model. As a proper extension of the Kolmogorov equation in an LES context, the Kármán–Howarth budget directly involves the balance of turbulent kinetic energy production and of the energy fluxes associated to the subgrid stresses. As pointed out in Meneveau (1994) and Meneveau & Katz (2000) in the context of isotropic turbulence, the Kármán–Howarth budget is a constraint to have the energy transfer rate towards small scales correctly reproduced. The *a posteriori* comparison with filtered DNS data (Piomelli, Moin & Ferziger 1988) will be used extensively to assess the quality of the different LESs. We will also deal with higher-order statistical properties such as the probability density function of longitudinal velocity increments and longitudinal structure functions. The latter have been analysed by Kang, Chester & Meneveau (2003) in an *a posteriori* comparison between filtered experimental data and the corresponding LES of decaying grid turbulence. For *a priori* tests in grid turbulence and in the wake of a cylinder, see Cerruti & Meneveau (2000).

The achievement of a flow with a uniform mean shear and homogeneous fluctuations has been challenging both experimentally and numerically. The first experiment by Rose (1966) showed that it was possible to realize a nearly homogeneous shear flow in an experimental device. A detailed characterization of the flow was provided by Champagne, Harris & Corrsin (1970). Harris, Graham & Corrsin (1977) and Tavoularis & Corrsin (1981*a*, *b*) extended the analysis further downstream using longer facilities. They found that both the turbulent intensities and the integral scale were increasing monotonically downstream while the Taylor scale remained substantially constant, see also the results by Rohr *et al.* (1988) in a water tunnel and by Tavoularis & Karnik (1989) and be Souza, Nguyen & Tavoularis (1995). On the numerical side, the first simulations in a confined box were performed by (Rogallo 1981). The numerical works by Rogers & Moin (1987) and Lee, Kim & Moin (1990), focused on vorticity dynamics under strong shear, were followed by a detailed discussion of the regeneration cycle of the vortical structures by Kida & Tanaka (1994). Experiments have been re-addressed recently to deal with the issue of small-scale isotropy recovery (see e.g. Garg & Warhaft 1998; Ferchichi & Tavoularis 2000). As a follow on, Shen & Warhaft (2000) introduced an active grid to achieve higher Reynolds numbers. Their flow featured an integral scale constant in the streamwise direction, a crucial achievement in view of our present investigation. With the integral scale comparable with the transverse dimension of the apparatus from the beginning, any downstream growth was inhibited. By that time, Pumir & Shraiman (1994) and

Pumir (1996) had performed extensive numerical simulations in a confined box and were able to reach a statistically stationary state. In this case, the growth of the integral scale was limited by the box size, with a strong resemblance of the findings of Shen & Warhaft (2000). The effect of confinement was further discussed by Gualtieri *et al.* (2002) and by Shumacher & Eckhardt (2000), who proposed an alternative to Rogallo's algorithm. A further extensive comparison between experiments and numerics can be found in Shumacher (2001) and Shumacher, Sreenivasan & Yeung (2003). More general observables – longitudinal structure functions, say (experiments by Jacob *et al.* 2004) – were favourably contrasted to LES data in a confined box (Casciola *et al.* 2005). As we see, the homogeneous shear flow has a long history and nowadays evidence has been accumulated that, under proper confinement, the flow attains a statistically stationary state, a condition which, combined with homogeneity, largely simplifies the statistical analysis.

After this historical note we are ready to describe the structure of the paper. Section 2 provides the background on the LES methodology. Section 3 illustrates the budget for the resolved kinetic energy. The scale-by-scale Kármán–Howarth budget is introduced in § 4 to contrast results for different filter-to-shear scale ratios against filtered DNS data. Finally, higher-order statistics is discussed in § 5 before drawing our main conclusions in § 6 which infers the implications for bounded flows.

2. Large-eddy simulation of the homogeneous shear flow

We consider a homogeneous turbulent shear flow in a confined box with an imposed mean velocity gradient S. The velocity field $\boldsymbol{v}$ is decomposed into mean U and fluctuation $\boldsymbol{u}$, $\boldsymbol{v} = U(x_2)\boldsymbol{e}_1 + \boldsymbol{u}$, where $U(x_2) = Sx_2$ is the mean flow, S the constant shear, $\boldsymbol{e_1}$ is the unit vector in the streamwise direction with x_2 the coordinate along the mean velocity gradient and x_3 spanwise. In the incompressible Navier–Stokes equations, $\nabla \cdot \boldsymbol{u} = 0$, written in terms of velocity fluctuations

$$\frac{\partial \boldsymbol{u}}{\partial t} = (\boldsymbol{u} \times \boldsymbol{\zeta}) - \nabla\pi + \nu\nabla^2\boldsymbol{u} - Sv\boldsymbol{e}_1 - U\frac{\partial \boldsymbol{u}}{\partial x_1}, \tag{2.1}$$

$\boldsymbol{\zeta}$ is the curl of $\boldsymbol{u}$, $v \equiv u_2$, π is the modified pressure which includes the fluctuating kinetic energy $u^2/2$, ν is the kinematic viscosity and the divergence of the Reynolds stress tensor – a tensor field constant in space in a homogeneous flow – vanishes. After the positions $\xi_1 = x_1 - U(x_2)t \quad \xi_2 = x_2 \quad \xi_3 = x_3 \quad \tau = t$ (Rogallo 1981), the momentum equation is rearranged as

$$\frac{\partial \boldsymbol{u}}{\partial \tau} = (\boldsymbol{u} \times \boldsymbol{\zeta}) - \nabla\pi + \nu\nabla^2\boldsymbol{u} - Sv\boldsymbol{e}_1, \tag{2.2}$$

where the convection operated by the linear mean profile has been absorbed in the transformation and the spatial derivatives are now expressed in ξ-variables. By assuming periodic fluctuations in ξ-space we achieve a homogeneous shear flow in x-space, where the mean shear is exactly constant and the fluctuations are homogeneous in a statistical sense. Clearly, the finite box confines the flow and limits the growth of the integral scale. In the issuing stationary state, the system is characterized by pseudo cyclic oscillations of the turbulent kinetic energy (Pumir 1996; Gualtieri *et al.* 2002; Yakhot 2003; Shumacher 2004). In this respect, despite an artificial flavour, ξ-periodicity is beneficial since it sets a perfectly controllable environment to analyse the statistics of shear-dominated fluctuations. It also enables the use of standard pseudospectral methods in ξ-space, with all the related advantages

of accuracy and efficiency they bring about both for the direct (DNS) and the large-eddy simulation (LES) of the flow.

The coarse graining of the field is achieved by convolution with a filter kernel G acting in x-space, which is spatially homogeneous with a compact support to ensure the commutation of spatial derivatives and filtering operator. The equation for the coarse-grained field $\bar{\boldsymbol{u}}$ follows after applying the filter,

$$\frac{\partial \bar{\boldsymbol{u}}}{\partial t} = (\overline{\boldsymbol{u} \times \boldsymbol{\zeta}}) - \nabla \bar{\pi} + \nu \nabla^2 \bar{\boldsymbol{u}} - S \bar{v} \boldsymbol{e}_1 - \overline{U \frac{\partial \boldsymbol{u}}{\partial x_1}}, \tag{2.3}$$

where, according to widespread use, the overbar denotes filtering. The term accounting for the convection of the mean field is split into two contributions

$$\overline{U \frac{\partial \boldsymbol{u}}{\partial x_1}} = U \frac{\partial \bar{\boldsymbol{u}}}{\partial x_1} - \frac{\partial \left(U \bar{\boldsymbol{u}} - \overline{U \boldsymbol{u}} \right)}{\partial x_1}, \tag{2.4}$$

where the last contribution on the right-hand side is periodic in ξ-space while the first one can be absorbed into Rogallo's transformation to yield

$$\frac{\partial \bar{\boldsymbol{u}}}{\partial \tau} = (\boldsymbol{h} + \boldsymbol{H}) - \nabla \bar{\pi} + \nu \nabla^2 \bar{\boldsymbol{u}} - S \bar{v} \boldsymbol{e}_1. \tag{2.5}$$

In (2.5), neither $\boldsymbol{h} = \overline{\boldsymbol{u} \times \boldsymbol{\zeta}}$ nor $\boldsymbol{H} = \partial (U \bar{\boldsymbol{u}} - \overline{U \boldsymbol{u}}) / \partial x_1$ have closed form in terms of $\bar{\boldsymbol{u}}$ alone, and must be modelled.

Among the available closure models, we have chosen one in the class of deconvolution methods, namely the approximate deconvolution method (ADM) (Stolz & Adams 1999; Stolz *et al.* 2001). Moreover, the model presents a single tunable constant χ_u which controls the relaxation term σ introduced below to enforce stability. Clearly this is one of the possible choices in the class of models based on the estimation of unresolved scales which have been considered by different authors (see e.g. Domaradsky & Saiki 1997; Guerts 1997; Domaradsky & Loh 1999; Guerts & Holm 2003; Mathew *et al.* 2003, 2006).

In the spirit of deconvolution approaches, the unknown field $\boldsymbol{u}$ is replaced in the unclosed terms $\boldsymbol{h}$ and $\boldsymbol{H}$ by the estimate $\boldsymbol{u} \simeq \boldsymbol{u}^* = Q_N * \bar{\boldsymbol{u}}$ obtained from the coarse-grained field via an approximate inverse filter $Q_N = \sum_{n=1}^{N} (I - G)^n \simeq G^{-1}$ (Stolz & Adams 1999). Here we use $N = 5$. Hence the approximately deconvolved terms are

$$\boldsymbol{h}^* = \overline{\boldsymbol{u}^* \times \boldsymbol{\zeta}^*}, \quad \boldsymbol{H}^* = \frac{\partial (U \bar{\boldsymbol{u}} - \overline{U \boldsymbol{u}^*})}{\partial x_1}, \tag{2.6}$$

and the LES equations read

$$\frac{\partial \bar{\boldsymbol{u}}}{\partial \tau} = (\boldsymbol{h}^* + \boldsymbol{H}^*) - \nabla \bar{\pi} + \nu \nabla^2 \bar{\boldsymbol{u}} - S \bar{v} \boldsymbol{e}_1 + \sigma, \tag{2.7}$$

where we have added the relaxation term σ. As they stand, the LES equations (2.7) are independent of the discretization procedure. In principle, we could define a filter cutoff length L_F and refine the grid by reducing the mesh size Δ until the modelled coarse-grained equation yields a convergent solution (Guerts & Frohlich 2002).

In fact, such, a grid-independent solution is hardly achieved in practice and the finite mesh size Δ enters beside L_F as an additional length scale in the discrete problem. It is on finite grids that the relaxation term $\sigma = -\chi_u (I - Q_N * G) * \bar{\boldsymbol{u}}$ (Stolz *et al.* 2001), may become crucial. Actually, the approximate inversion of the filter is reasonably accurate in the range $\omega = k\Delta \leqslant \omega_F$, where k is the wavenumber and ω_F the nominal dimensionless cutoff wavenumber of the filter such that $|\hat{G}(\omega_F)| = 1/2$

(a hat denotes here the Fourier transform in x-space, and $\omega_F = 2\pi\Delta/L_F$). Hence, for $\omega \leqslant \omega_F$, $\hat{G}(\omega) \simeq 1$ and $\hat{Q}_N(\omega) \simeq 1$, so that $\hat{\sigma}(\omega) \simeq 0$, i.e. the resolved scales are untouched by the artificial dumping. On the contrary, in the high-wavenumber range of the grid $\omega_F \leqslant \omega \leqslant \omega_\Delta$ a non-vanishing energy transfer towards the scales beyond grid resolution, $\omega > \omega_\Delta$, calls for an additional, purely dissipative term purposely designed to remove energy from the high-wavenumber end of the spectra. Here, in general, we have to expect $\hat{\sigma}(\omega) \neq 0$. This kind of reasoning is recast in a more rational form (Carati *et al.* 2001; Winckelmans, Wray & Jeanmart 2001). LES can be obtained from the Navier–Stokes equations by applying a smooth filter and a discretization operator. Two different contributions appear then in the subgrid stresses. One, the resolved subgrid stresses, can in principle be recovered exactly from the filtered velocity field when invertible filters are used. In our case, the approximate deconvolution provides an estimate of this part. The other contribution, the unresolved stresses, is due to the discretization which irreversibly destroys all the information below the grid spacing. There is no chance of recovering these stresses in purely mathematical terms. In the context of the ADM, the unresolved stresses are modelled via the purely dissipative relaxation term. As shown later, it becomes substantially irrelevant when the resolved subgrid stresses fall short of accounting for the entire amount of stress required by the simulation. In any case, the relaxation term introduced above is not the only possibility for modelling the unresolved stresses in a deconvolution model. An eddy-viscosity model can work as well, see Carati *et al.* (2001) and the application in a channel flow by Gullibrand & Chow (2003).

Before discussing the simulations and the quality of the turbulence, let us provide a few more details on the numerics. The geometry of the flow naturally calls for Fourier-based pseudospectral algorithms in ξ-space where the modified pressure is eliminated via the classical Fourier-space projector, with the advantage that the high accuracy prevents numerical errors from overwhelming the subgrid model (see Ghosal 1996; Chow & Moin 2003). Time advancement is achieved through a fourth-order low-storage Runge–Kutta method. A re-meshing procedure, whereby the box is mapped back to its initial unskewed configuration, is periodically applied to mitigate the distortion of the grid in physical space, as originally suggested by Rogallo (see Gualtieri *et al.* 2002 and references therein). We stress that aliasing errors can be induced in principle by the moving grid. To avoid spurious contamination of the resolved range, every time the box is re-meshed, dealiasing is performed concurrently. Care is taken to ensure that only an insignificant fraction of the energy is filtered-out in this way when the code is operated in DNS mode, which is of course the case that is potentially more sensitive to this issue, since in LES the explicit filtering already keeps the situation under control. The Appendix and figure 1 give further information on the filtering procedure and the main properties of the filters.

3. Low-order statistics

Several LES simulations which differ for filter scale L_F, and nominal Reynolds number $Re_N = SL_y^2/\nu$ – L_y is the box dimension in the shear direction – are addressed to discuss the quality of the large-scale statistics. In all cases, the subgrid resolution L_F/Δ is held fixed. Owing to filtering, below L_F the field is smooth. Hence the subgrid resolution is a measure of the accuracy achieved in solving the filtered equations, i.e. we recover their exact solution when Δ becomes sufficiently smaller than L_F. Two values of the Reynolds number are considered, namely $Re_N \simeq 10\,000$ and $20\,000$. The

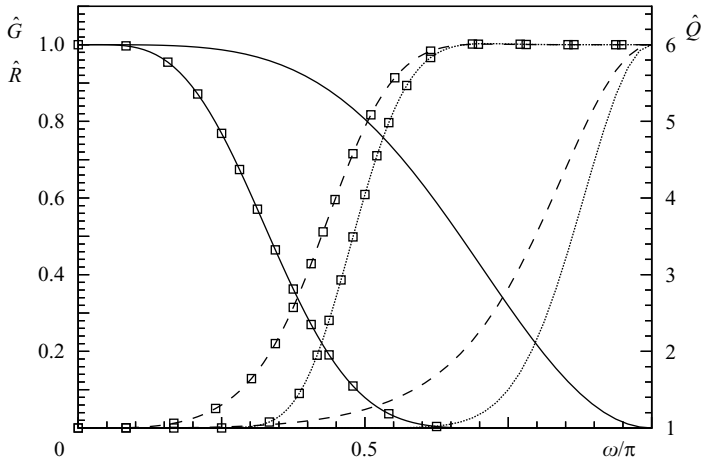

FIGURE 1. Fourier transform of the primary filter $\hat{G}$ (solid lines), of the approximate inverse $\hat{Q}_N$ (dashed lines) and of the secondary filter $\hat{R} = \hat{I} - \hat{Q}_N \hat{G}$ (dotted lines) as a function of the non-dimensional wavenumber $\omega = k\Delta/\pi$. Lines with symbols correspond to the filter used in the direction of the mean shear. Note the different non-dimensional cutoff wavenumber which correspond, to a physical length scale L_F uniform in all the three spatial directions.

shear S and and the box dimension L_y in the direction of the shear are kept constant, together with all the other geometrical (e.g. aspect ratios) and numerical (e.g. time step, re-meshing frequency, dealiasing procedure) parameters.

The basic data set consists of three simulations at $Re_N \simeq 10\,000$, ordered by increasing cutoff length (i.e. $L_{F1} < L_{F2} < L_{F3}$) and denoted by LES_1, LES_2 and LES_3, respectively. We have also performed an extensive analysis at larger Reynolds number ($Re_N \simeq 20\,000$) to check the sensitivity of the subgrid model to variations in the relaxation parameter χ_u for two choices of the filter scale, $L_{F1} < L_{F2}$. These simulations are denoted with the superscript 'H'. Table 1 provides a summary of the data set and the main global features for each case.

Beside the large-eddy simulations, two fully resolved DNS were run to obtain real Navier–Stokes turbulence in corresponding physical conditions. DNS fields have been *a posteriori* filtered to provide reference filtered data. The corresponding data sets are denoted by DNS_1, DNS_2, DNS_3 and DNS_1^H, DNS_2^H, for the lower and higher Reynolds number, respectively. The first five entries in table 1 provide information on the coarse-grained DNS data sets for comparison with corresponding LES. The parameters of the two DNS are given in table 2.

3.1. *Turbulence scales*

As is well known, the shear scale $L_S = \sqrt{\epsilon/S^3}$, where ϵ is the mean turbulent kinetic energy dissipation rate, plays a fundamental role. Within the inviscid range above the Kolmogorov scale $\eta = (\nu^3/\epsilon)^{1/4}$ and below the integral scale L_0, L_S singles out the scales $L_S < r < L_0$ where turbulence is driven by the production, from those $\eta < r < L_S$ where the inertial energy transfer is established to give rise eventually to the dissipative range. However, there are other characteristic length scales in turbulence. A classical example of intermediate scale is the Taylor microscale $\lambda^2 = 15\nu u_{rms}^2/\epsilon$, here conventionally defined in terms of the streamwise fluctuations $u_{rms} = \sqrt{\langle u_1^2 \rangle}$, where

Run	L_F	L_F/L_S	$\bar{u}_{rms}$	$\langle\bar{u}_1\bar{u}_2\rangle$	Π	$\bar{\epsilon}_v$	ϵ^*_{sgs}	ϵ_{rel}	ϵ_{da}	ST_{max}
DNS_1	0.59	0.82	0.52	−0.133	0.066	0.020	0.046	–	–	–
DNS_2	0.79	1.10	0.50	−0.128	0.064	0.012	0.052	–	–	–
DNS_3	1.05	1.46	0.44	−0.102	0.051	0.008	0.043	–	–	–
DNS_1^H	0.59	0.82	0.49	−0.120	0.060	0.010	0.050	–	–	–
DNS_2^H	0.79	1.10	0.42	−0.092	0.046	0.009	0.053	–	–	–
LES_1	0.59	0.82	0.51	−0.133	0.066	0.022	0.042	0.4×10^{-4}	0.2×10^{-2}	7800
LES_2	0.79	1.10	0.45	−0.106	0.053	0.014	0.037	0.8×10^{-4}	0.2×10^{-2}	7600
LES_3	1.05	1.46	0.37	−0.071	0.035	0.008	0.025	0.2×10^{-2}	–	2300
$LES_1^H(a)$	0.59	0.82	0.50	−0.120	0.060	0.010	0.038	0.7×10^{-2}	0.5×10^{-2}	2000
$LES_1^H(b)$	0.59	0.82	0.47	−0.115	0.057	0.012	0.040	0	5.5×10^{-3}	2000
LES_2^H	0.79	1.10	0.43	−0.092	0.046	0.007	0.029	0.8×10^{-2}	2×10^{-3}	4000

TABLE 1. Summary of coarse-grained DNS and LES. The cutoff length scale L_F of the filter is constant in the three Cartesian directions, while the grid spacing changes. The cutoff wavenumber, once made dimensionless with the appropriate grid spacing, is $2\pi\Delta^{(x/z)}_{LES}/L_F = 2/3\pi$ in both the streamwise and the spanwise direction and $2\pi\Delta^{(y)}_{LES}/L_F = 1/3\pi$ along the mean gradient, see figure 1. The resolutions of the four LES are $64\times64\times32$ (LES_1 and LES_1^H), $48\times48\times24$ (LES_2) and $36\times36\times18$ (LES_3). The corresponding coarse-grained DNS are denoted as DNS_1, DNS_2, DNS_3 and DNS_1^H, DNS_2^H. The viscous dissipation associated to the resolved (LES) or to the coarse-grained (filtered DNS) field is denoted by $\bar{\epsilon}_v$. Column ϵ^*_{sgs} gives the amount of dissipation ascribed to the explicit subgrid stresses. It corresponds to the total subgrid dissipation for the coarsened DNS fields while for LES, additional energy draining is due to the relaxation term, ϵ_{rel}, and to dealiasing, ϵ_{da}. Within statistical accuracy, the sum ϵ of all terms balances the resolved production $\epsilon = \Pi = -S\langle\bar{u}_1\bar{u}_2\rangle$. This allows us to estimate by difference the energy dissipated in the LES via dealiasing. For LES_3, ϵ_{da}, comparable in magnitude with the confidence interval for the average production Π, is not reported. The relaxation parameter χ_u was systematically varied in the range $0 < \chi_u < 2000u_\tau/L_y$ where the equivalent friction velocity is $u_\tau = \sqrt{\nu S - \langle u_1u_2\rangle}$. The data shown in the table correspond to the upper limit. Last column: total integration time of the LES simulations.

Run	Re_N	Re_λ	S^*	u_{rms}	$\langle u_1u_2\rangle$	$\Pi=\epsilon$	L_S	λ	η	ST_{max}
DNS	9870	100	7	0.52	−0.118	0.059	0.72	0.37	0.02	870
DNS^H	19740	150	7	0.52	−0.118	0.059	0.70	0.27	0.01	340

TABLE 2. Summary of DNS simulations. The Reynolds number is defined as $Re = SL_y^2/\nu$, the box size is $L_x\times L_y\times L_z = 4\pi\times2\pi\times2\pi$. Resolution: DNS $256\times256\times128$ Fourier modes. DNS^H $384\times384\times192$ Fourier modes. The Taylor microscale Reynolds number is $Re_\lambda = u_{rms}\lambda/\nu$ where $u_{rms} = \sqrt{1/3\langle u_iu_i\rangle}$ and $\lambda^2 = 15\nu u^2_{rms}/\epsilon$ with ϵ the mean turbulent kinetic energy dissipation rate. The shear parameter is $S^* = 3u^2_{rms}S/\epsilon = (L_0/L_S)^{2/3}$, where $L_0 = (3u^2_{rms})^{3/2}/\epsilon$ is the integral scale, $L_S = \sqrt{\epsilon/S^3}$ the shear scale and $\eta = (\nu^3/\epsilon)^{1/4}$ the Kolmogorov scale. Last column: total integration time of the simulations.

the angular brackets denote ensemble averaging. It is worth stressing that L_S/L_0 is a Reynolds-number-independent quantity, set by the large scales of the flow, as is immediately realized from the turbulent kinetic energy balance $\epsilon = -\langle uv\rangle S$. On the contrary, the Taylor microscale λ depends on the small scales, as is understood from the usual scaling argument $Re_\lambda = u_{rms}\lambda/\nu \propto (u_{rms}L_0/\nu)^{1/2}$. This simple reasoning is important for LES. At the fixed the subgrid resolution L_F/Δ, the basic parameter which affects the resolved scales is the filter cutoff length L_F. As the nominal

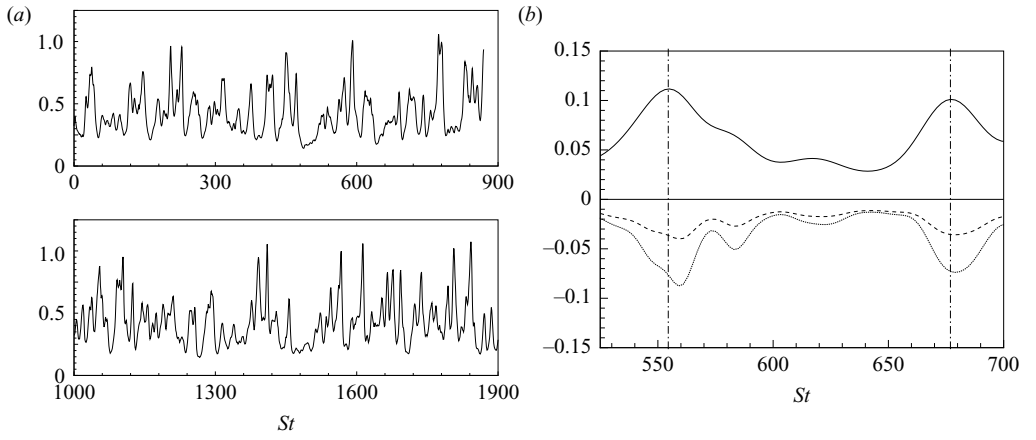

FIGURE 2. (*a*) Time history of the turbulent kinetic energy. Top panel: DNS. Bottom panel: LES. (*b*) Production of turbulent kinetic energy (solid line), resolved dissipation (dashed line) and subgrid dissipation (dotted line).

Reynolds number increases, we expect the large scales soon to reach a Reynolds-number-independent behaviour with viscous effects confined below λ, i.e. further and further away from the resolved scales above L_F. This rules out the possibility that *a posteriori* filtered data could show a dependence on the Taylor microscale, unless viscous effects are directly called into play, say by the no-slip condition in regions very close to a solid wall. Hence, if L_F/Δ is large enough to have reasonable numerical accuracy and the Reynolds number is not too small, a well-designed subgrid model should yield large-scale fluctuations which depend on the single parameter L_F/L_S.

3.2. *Statistically stationary state*

Let us turn our attention to the numerical results. In this system the integral scale cannot exceed the box size (Gualtieri *et al.* 2002). This leads to a statistically stationary state characterized by a cyclic growth and depletion of turbulent kinetic energy, as discussed by Pumir (1996) and Shumacher & Eckhardt (2000). The same behaviour is reproduced by the LES, where the subgrid energy dissipation rate plays a crucial role in the equation for the spatially averaged resolved turbulent kinetic energy

$$\frac{\partial}{\partial t}\left[\frac{\bar{\boldsymbol{u}}^2}{2}\right] = -S[\bar{u}_1\bar{u}_2] - 2\nu[\bar{s}_{ij}\bar{s}_{ij}] + [\tau_{ij}\bar{s}_{ij}] + [\sigma_i\bar{u}_i], \tag{3.1}$$

where square brackets denote spatial average, $\bar{s}_{ij}$ is the resolved strain rate, τ_{ij} the subgrid stresses and σ_i the relaxation stress.

A small portion of the time history of the resolved turbulent kinetic energy for case LES_1 (see table 1) is reproduced in figure 2. The balance between production, resolved and subgrid dissipation is achieved as a time average over the aforementioned pseudocyclic behaviour. The bursting frequency of these self-sustained oscillations was shown to be independent of the box size and controlled by the inviscid time scale S^{-1} (Gualtieri *et al.* 2002). Yakhot (2003) concluded that, in the large-strain limit, this dynamical system is characterized by self-sustained nonlinear oscillations with size-independent period. Apparently, LES correctly reproduces the sequence of large-scale essentially inviscid events which give rise to the cycles (figure 2).

3.3. *Reynolds stresses*

If we were to judge the quality of a large-eddy simulation from a single observable, a candidate would be the shear component of the Reynolds stress, $-\langle u_1 u_2 \rangle$. Since the flow is statistically homogeneous and stationary, common practice demands that we estimate the averages from the mean values taken simultaneously in space and in time – temporal mean values are indicated by a tilde, $-\langle u_1 u_2 \rangle \simeq -[\widetilde{u_1 u_2}]$.

Clearly, there is no way to reconstruct the exact Reynolds stress from an LES. Instead we access the resolved Reynolds stresses, whose shear component $-\langle \overline{u}_1 \overline{u}_2 \rangle$ can be directly compared to the correspondingly filtered DNS. The shear scale in both our DNS is about $L_S = 0.72$ (table 2) since the Reynolds shear stress is $-\langle u_1 u_2 \rangle = 0.118$ in either case and both flows are in equilibrium $-S\langle u_1 u_2 \rangle = \epsilon = 0.059$. From table 1, as the filter bandwidth increases, an increasingly significant part of Reynolds stress and production in the DNS occurs below the filter cutoff. Hence, most quantities are progressively underestimated by the filtered fields, e.g. the coarse grained production $\Pi = -S\langle \bar{u}_1 \bar{u}_2 \rangle$ – more properly the production associated with the coarse grained field – differs from the DNS by almost 14 % in the case of the most severe filter corresponding to DNS_3. Similar trends are displayed by the other quantities. Compared to unfiltered data, Reynolds-stress-related quantities first increase – DNS_1 – to decrease afterwards monotonously with the filter bandwidth – DNS_2 and DNS_3. This behaviour is easily understood from the Fourier decomposition of the shear stress, the cospectrum $\langle \hat{u}_1 \hat{u}_2 \rangle$ (not shown), which, being negative at large scales, becomes positive at high wavenumbers. The same trend is followed by the resolved production Π and by the overall dissipation ϵ of the exact coarse-grained field, which is defined as the sum of the resolved dissipation $\overline{\epsilon}_v = 2\nu \overline{s}_{ij} \overline{s}_{ij}$ and the subgrid energy transfer $\epsilon_{sgs} = \langle \tau_{ij} \overline{s}_{ij} \rangle$, where the exact subgrid stress is

$$\tau_{ij} = \overline{u_i u_j} - \overline{u}_i \overline{u}_j, \tag{3.2}$$

and $\overline{s}_{ij}$ is the filtered deformation velocity. The fluctuation intensity of the coarse-grained field $\overline{u}_{rms} = \sqrt{1/3 \langle \overline{u}_i \overline{u}_i \rangle}$ provides analogous indications.

Whatever the behaviour, the filtered DNS results we have discussed so far are exact, a matter of consistently applying a well-defined filtering procedure to the fully resolved fields. The interesting comparison is between 'exact' *a posteriori* filtered data and LES simulations, where we introduce the inaccuracy of the subgrid model (table 1). A filter scale only 10 % above the shear scale results in approximately 20 % error in the resolved Reynolds stresses, see LES_2 in comparison with DNS_2, and, in general as L_F increases above L_S a progressive misprediction of the large-scale energy production rate occurs in the LES, see LES_3 *vs.* DNS_3. Instead, when $L_F \simeq L_S$, we observe an almost perfect agreement between filtered DNS and LES, compare DNS_1 and LES_1 in table 1. The same trend is observed also for the higher Reynolds number, $Re_N = 20\,000$, provided $L_F < L_S$. In this case, the relaxation parameter χ_u must be tuned properly in the ADM and more generally the unresoved stresses, to recover the turbulent kinetic energy production rate, as we will discuss in more detail in § 3.4.

Consistently with our initial conjecture, in the context of the ADM as soon as the filtering occurs above the shear scale, $L_F > L_S$, the model becomes unable to agree with the filtered DNS, see case LES_2^H in the table, where the reasonable value of the production occurs by chance in a general framework of bad values for other statistical observables such as the energy spectra, as will be discussed in § 3.5

3.4. *Turbulent kinetic energy budget*

As anticipated, the subgrid stresses are given in the ADM model by two contributions. An explicit term,

$$\tau^*_{ij} = \overline{u^*_i u^*_j} - \overline{u}_i \overline{u}_j, \tag{3.3}$$

which, a part from the deconvolution of the resolved field implied by the asterisk, corresponds to the exact subgrid stresses (3.2), plus the additional dissipative contribution σ provided by the relaxation term, whose underlying stresses τ_σ would be given by the equation $\nabla \cdot \tau_\sigma = \sigma$. In fact, in a fully dealiased spectral method, the dynamics is also affected by 'virtual' subgrid stresses associated to dealiasing. The explicit form taken either by τ_σ or by the 'virtual' stresses is of no practical relevance. The amount of resolved kinetic energy they drain from the resolved field is, however, important. In such conditions, in a homogeneous stationary ensemble, the balance of resolved turbulent kinetic energy becomes

$$\Pi = \overline{\epsilon}_v + \epsilon_{sgs} = \overline{\epsilon}_v + \epsilon^*_{sgs} + \epsilon_{rel} + \epsilon_{da}, \tag{3.4}$$

where the total subgrid energy transfer ϵ_{sgs} is the sum of the transfer operated by the explicit subgrid stresses, $\epsilon^*_{sgs} = \langle \tau^*_{ij} \overline{s}_{ij} \rangle$, of the energy drain due to the relaxation term $\epsilon_{rel} = \langle \sigma_i \overline{u}_i \rangle$ and of the energy removed on average by the dealiasing procedure ϵ_{da}.

In table 1, the balance (3.4) is addressed term by term for both values of the nominal Reynolds number we have considered.

Let us first address the smaller-Reynolds-number case, $Re_N \simeq 10\,000$. When LES and filtered DNS data agree – LES_1 *vs.* DNS_1, $L_F/L_S \simeq 0.8$ – filtering occurs below the shear scale and the explicit subgrid stresses account for all the subfilter energy transfer. A small fraction – order of 3 % – of the dissipation in the resolved scale is due to dealiasing. Only an insignificant part of dissipation – less then 0.06 % – is generated by the relaxation term. In these conditions, if the artificial relaxation term is turned off by putting $\chi_u = 0$, no appreciable change is observed in the solution. If we move the filter cutoff a little above the shear scale – as in LES_2 and DNS_2, $L_F/L_S = 1.1$ – a certain inaccuracy in the LES begins to emerge and modelling errors tend to become significant, namely the intensity in the resolved fluctuations is underestimated by about 10 % while Reynolds shear stress and resolved production are wrong by more then 17 %. Still the energy drained by the artificial relaxation term is negligible and dealiasing gives a small contribution. Increasing further the filter scale – LES_3 *vs.* DNS_3 – leads to incorrect results, e.g. the resolved Reynolds shear stress is missed by about 30 %. In these conditions the artificial relaxation and dealiasing contribute significantly, and the results are bound to depend on the value of the tunable constant χ_u.

When the Reynolds number increases, $Re_N = 20\,000$, the interaction between subgrid and resolved scales above the nominal filter cutoff is no longer negligible and the unresolved stresses, vanishingly small at $Re_N = 10\,000$, are now substantial. In these conditions, the resolved stresses cannot account for the total energy flux. It follows that the additional energy draining due to the relaxation term becomes important in 'real LES' conditions.

In fact, for the $LES^H_1(a)$ at $Re_N = 20\,000$, the grid is sufficiently fine to resolve the shear scale L_S and $L_F < L_S$. At this Reynolds number, a significant activity occurs below the grid cutoff Δ of the LES, as shown by the DNS data. The balance (3.4) (table 1) confirms that the production of the turbulent kinetic energy is captured well by the LES. However, the resolved stresses do not give the reason for the entire amount of subfilter energy transfer. Its correct value is recovered only when adding

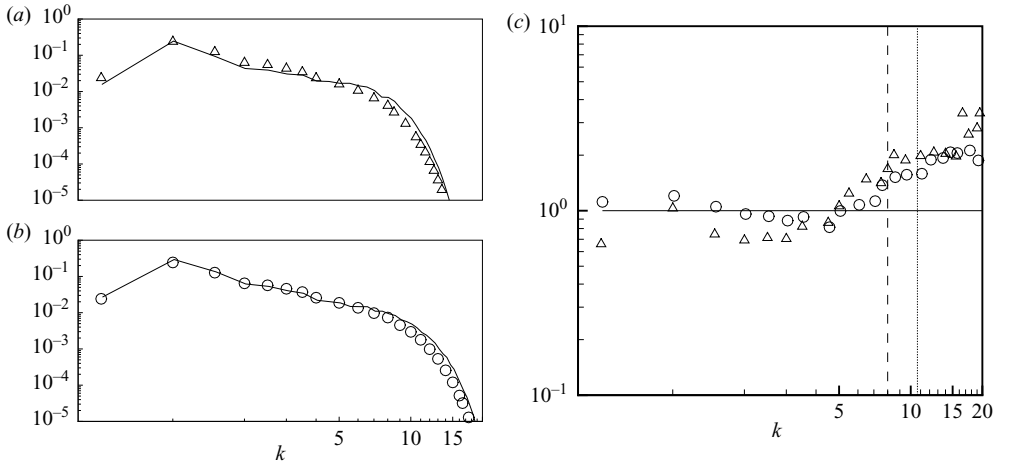

FIGURE 3. (a, b) Energy spectra for LES and filtered DNS data. Top panel: $L_F/L_S = 1.10$, LES_2 (line) *vs.* DNS_2 (triangles). Bottom panel: $L_F/L_S = 0.82$, LES_1 (line) *vs.* DNS_1 (circles). (c) Same data plotted as ratio of LES to filtered DNS spectra, $L_F/L_S = 0.82$ (circles) and $L_F/L_S = 1.10$ (triangles). The filter cutoff is indicated by the vertical dashed and dotted line at $k_F = 8$ and $k_F = 10.7$, respectively.

the contributions of the relaxation term and dealiasing. The relaxation term provides 10 % of the total energy flux and it is crucial. Switching the relaxation parameter off, completely destroys the accuracy, see case $LES_1^H(b)$. Actually, $LES_1^H(a)$ with $\chi_u = 100$ compares favourably with DNS_1^H whereas $LES_2^H(b)$ with $\chi_u = 0$ does not. An extensive sensitivity analysis to changes in χ_u (not shown) indicates that its precise value is not critical and $\chi_u = 150$ works as well. Compared with $Re_N = 10\,000$, doubling the Reynolds number with the same grid, shear and filter scale enhances the relaxation term by two orders of magnitude, LES_1 *vs.* LES_1^H.

3.5. *Energy spectra*

In LES, accurate single-point observables do not necessarily guarantee the correct energy distribution in wavenumber, see for example the comments in Jimenez & Moser (2000), since the modelled subgrid stresses may still alter the resolved scales. Spectra from LES are shown in figure 3 for our moderate-Reynolds-number case. As far as $L_F < L_S$, they are consistent with DNS. As soon as $L_F > L_S$, the solution becomes inadequate in terms of both subgrid dissipation and spectrum, as confirmed by the resolved-to-exact spectral density ratio (figure 3*c*). The alteration of the spectra, just perceivable at $L_F/L_S = 1.1$, becomes substantial at $L_F/L_S = 1.46$. Figure 4 repeats the analysis at $Re_N = 20\,000$. The alteration is apparent for case LES_2^H where $L_F > L_S$. Also at this Reynolds number everything works well when $L_F < L_S$ and the constant in the relaxation term is properly tuned, as for case $LES_1^H(a)$. However, with this relatively coarse grid, turning off the relaxation term irremedably deteriorates the spectra, case $LES_1^H(b)$, see figure 4(b) where the energy spectra are reported in a linear scale to appreciate better the largest resolved scales.

4. The Kármán–Howarth budget

In a homogeneous shear flow, the energy content of the different scales is set by a delicate balance between production and transfer. A poor reproduction of either one

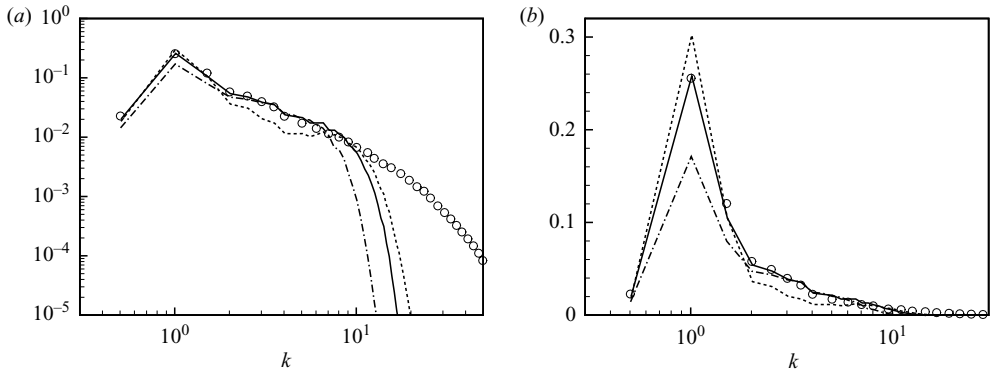

FIGURE 4. (*a*) Energy spectra for LES (lines) and DNS (symbols) at $Re_N \simeq 20\,000$. LES_2^H (dash-dotted line) corresponding to $L_F/L_S = 1.10$ and $Xu = 150$. $LES_1^H(a)$ (solid line) with $L_F/L_S = 0.82$ and $Xu = 150$. $LES_1^H(b)$ (dotted line) with $L_F/L_S = 0.82$ and $Xu = 0$. (*b*) Same spectra in linear scale; symbols as in (*a*).

results in erroneous equilibrium conditions at each scale, and this inevitably leads to the wrong shapes for the spectra.

In isotropic conditions, the Kármán–Howarth equation describes the Richardson energy cascade and reduces to the celebrated Kolmogorov four-fifths law. For anisotropic flows, a generalization thereof allows for the evaluation of the nonlinear energy flux and of the production of turbulent kinetic energy related to each scale (Casciola *et al.* 2003). In the present context, it is crucial to take into consideration the subgrid stresses both in the exact and in the modelling context. The analysis is focused on the central processes of turbulent kinetic energy production and transfer towards small scales. For a related analysis in isotropic conditions see Meneveau (1994).

The principal manipulations helpful in deriving the balance equation are reviewed below, to offer a self-contained discussion while at the same time taking the chance of commenting on the effect of filtering and modelling.

Let us rewrite in a slightly more general form the filtered Navier–Stokes equation for the fluctuating field

$$\frac{\partial \overline{u}_i}{\partial t} + \overline{u}_k \frac{\partial \overline{u}_i}{\partial x_k} = -\frac{1}{\rho}\frac{\partial \overline{p}}{\partial x_i} - U_k \frac{\partial \overline{u}_i}{\partial x_k} - \overline{u}_k \frac{\partial U_i}{\partial x_k} + \nu \frac{\partial \overline{u}_i}{\partial x_k \partial x_k} - \frac{\partial}{\partial x_k}(\tau_{ik} + T_{ik}) + \sigma_i, \qquad (4.1)$$

where the homogeneous mean flow is $U_k = (\partial U_k/\partial x_j)_0 x_j$, and p is the pressure. When the only non-vanishing component of the constant gradient is $(\partial U_1/\partial x_2)_0 = S$, we recover the shear flow. Equation (4.1) reduces to a simple filtering when $\tau_{ik} = \overline{u_i u_k} - \overline{u}_i \overline{u}_k$, $T_{ik} = \overline{u_i U_k} - \overline{u}_i U_k$ and $\sigma_i = 0$. Alternatively, after setting $\tau_{ik} = \overline{u_i^* u_k^*} - \overline{u}_i \overline{u}_k$, $T_{ik} = \overline{u_i^* U_k} - \overline{u}_i U_k$ and taking the appropriate expression for the relaxation term σ_i we recover an equation equivalent to (2.7).

We derive first an equation for the two-point correlation $\langle \overline{u}_i \overline{u}'_j \rangle$ where a prime denotes the velocity evaluated at $\boldsymbol{y} = \boldsymbol{x} + \boldsymbol{r}$ following the procedure reported in Casciola *et al.* (2003). After taking the trace of the equation for the two-point correlation rearranging certain contributions in terms of velocity increments – $\delta U_k = U'_k - U_k$ for the mean flow and $\delta \overline{u}_i = \overline{u}'_i - \overline{u}_i$ for the coarse-grained fluctuating field – we introduce the two-point-averaged tensors $\tau_{ik}^\dagger = \tau'_{ik} + \tau_{ik}$ and $T_{ik}^\dagger = T'_{ik} + T_{ik}$ to obtain the equation for the turbulent scale energy of the coarse-grained field

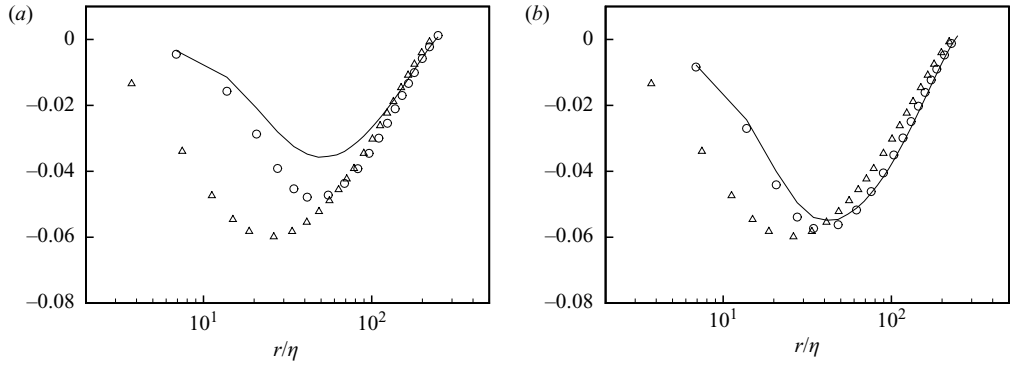

FIGURE 5. $Re_N = 10\,000$. Transfer term in the Kármán–Howarth budget S_3^{tr}/r *vs.* separation. (*a*) $L_F/L_S = 1.10$, LES_2 (line) *vs.* DNS_2 (circles). (*b*) $L_F/L_S = 0.82$, LES_1 (line) *vs.* DNS_1 (circles). Triangles provide unfiltered DNS data for comparison.

$\langle \delta\overline{u}^2 \rangle = \langle \delta\overline{u}_i \delta\overline{u}_i \rangle$. Finally, the equation is spatially averaged on a ball $\mathscr{B}_r$ of radius r leading to the Kármán–Howarth equation,

$$\begin{aligned} &\frac{1}{4\pi r^2} \oint_{\partial B_r} \langle \delta\overline{u}^2 \delta\overline{u}_k \rangle n_k + n_1 n_2 Sr \langle \delta\overline{u}^2 \rangle \, \mathrm{d}S_r + \frac{2}{4\pi r^2} \oint_{\partial B_r} \langle (\tau_{ik}^{\dagger} + T_{ik}^{\dagger}) \delta\overline{u}_i \rangle n_k \, \mathrm{d}S_r \\ &\quad = \tfrac{4}{3} S \langle \overline{u}_1 \overline{u}_2 \rangle r - \frac{2S}{4\pi r^2} \int_{B_r} \langle \delta\overline{u}_1 \delta\overline{u}_2 \rangle \, \mathrm{d}V_r - \tfrac{4}{3} \langle \sigma_i \overline{u}_i \rangle r \\ &\qquad + \frac{2}{4\pi r^2} \oint_{\partial B_r} \langle \delta\sigma_i \delta\overline{u}_i \rangle \, \mathrm{d}V_r + \frac{\mathrm{d}}{\mathrm{d}r} \left(\frac{2\nu}{4\pi r^2} \oint_{\partial B_r} \langle \delta\overline{u}^2 \rangle \, \mathrm{d}S_r \right), \end{aligned} \tag{4.2}$$

either for the coarse-grained or for the LES modelled field, depending on the definitions of τ_{ik}, T_{ik} and σ_i – remember that 1 and 2 are the directions of mean stream and mean gradient respectively, while $\boldsymbol{n}$ is the outward normal to the ball. As we see from (4.2), several mechanisms are involved in the balance of the scale energy of the coarse-grained field. The first term in the left-hand side,

$$S_3^{tr} = \frac{1}{4\pi r^2} \oint_{\partial B_r} \langle \delta\overline{u}^2 \delta\overline{u}_k \rangle n_k + n_1 n_2 Sr \langle \delta\overline{u}^2 \rangle \, \mathrm{d}S_r, \tag{4.3}$$

is a generalized third-order structure function, see the classical Kolmogorov four-fifths law where it is reshaped in terms of longitudinal structure function, $S_3^{tr} \propto \langle \delta u_{\parallel}^3 \rangle$. This term quantifies the energy flux across scale r, i.e. the energy which feeds the scales smaller than r. Here we are dealing with the filtered field, and the flux is due to the nonlinear self-advection and to the mean shearing of the coarse-grained fluctuations.

S_3^{tr} is plotted in figure 5, where LES data at $Re_N = 10\,000$ (lines) are contrasted against corresponding filtered DNS data (circles) for *a posteriori* comparison. The figure also shows the same term taken from the fully resolved DNS (triangles), the same as (4.3) except from filtering, i.e. now applied to the fine-grained field u rather than to $\overline{u}$. As it should, filtering changes the transfer term substantially – circles *vs.* triangles in the figure. The difference is significant in the intermediate range of scales, where the transfer term contributes the most. Concerning modelling (lines *vs.* circles), as the filter cutoff scale is appreciably larger than the shear scale, the accuracy of our LES model in reproducing the energy flux is poor, see figure 5(*a*). The decrease of L_F below L_S (figure 5*b*) considerably enhances the predictive power of LES for this rather delicate observable, which now approximates the exact values well.

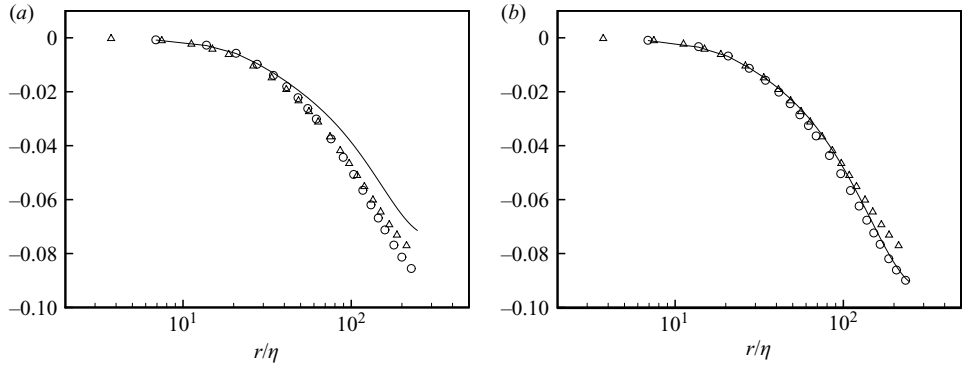

FIGURE 6. $Re_N = 10\,000$. Production term in the Kármán–Howarth budget S_3^{pr}/r *vs.* separation. (*a*) $L_F/L_S = 1.10$, LES_2 (line) *vs.* DNS_2 (circles). (*b*) $L_F/L_S = 0.82$, LES_1 (line) *vs.* DNS_1 (circles). Unfiltered DNS data are also plotted (triangles).

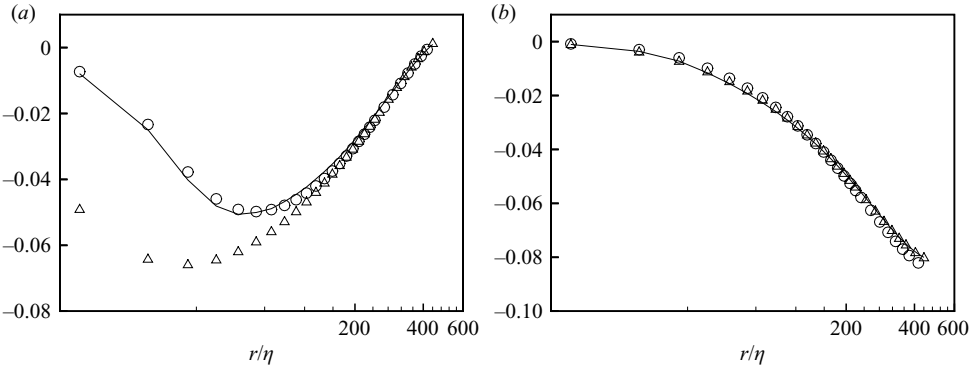

FIGURE 7. $Re_N = 20\,000$. (*a*) Transfer term in Kármán–Howarth budget S_3^{tr}/r *vs.* separation. (*b*) Production term S_3^{pr}/r. $LES_1^H(a)$ (lines) *vs.* DNS_1^H (circles). Unfiltered DNS correspond to the triangles.

The other relevant mechanism in shear turbulence is the production of turbulent kinetic energy. In the scale energy balance it is described by the term

$$S_3^{pr} = \frac{2S}{4\pi r^2} \int_{B_r} \langle \delta\bar{u}_1 \delta\bar{u}_2 \rangle \, \mathrm{d}V_r, \tag{4.4}$$

which is plotted in figure 6 for the available data. Also in this case, a perfect agreement with filtered DNS data is observed when $L_F < L_S$. On figure 6(*a*) $L_F > L_S$, the modelling error induces a discrepancy with the exactly filtered data (lines *vs.* circles) which largely overcomes the effect of filtering itself (circles *vs.* triangles). In figure 6(*b*) we see how the LES data approach the filtered DNS results, reproducing the expected difference with the fully resolved DNS production. Here the effect of pure filtering is felt strongly on the large scales, where production is the dominating phenomenology.

Figure 7(*a*) shows S_3^{tr} and figure 7(*b*) shows S_3^{pr} at $Re_N = 20\,000$. At this higher value of the Reynolds number, the relaxation term is significant. Nevertheless resolved energy flux and production is in excellent agreement with DNS data as soon as $L_F < L_S$.

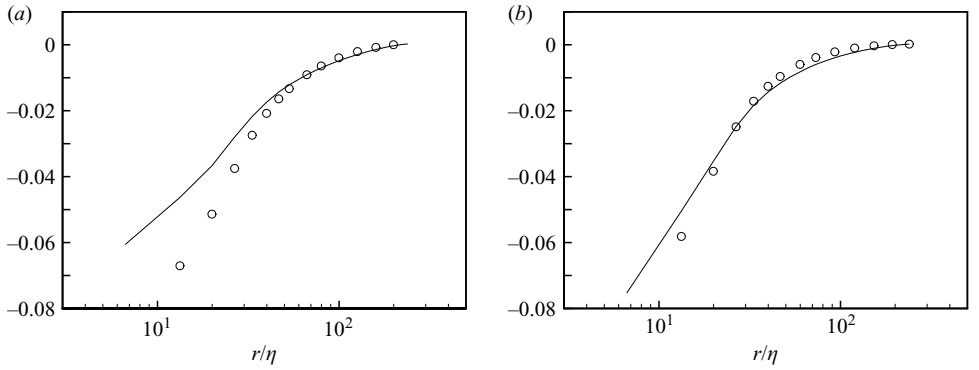

FIGURE 8. $Re_N = 10\,000$. Compensated subgrid fluxes and viscous terms in the Kármán–Howarth budget against separation. (*a*) $L_F/L_S = 1.10$, LES_2 (line) *vs.* DNS_2 (circles). (*b*) $L_F/L_S = 0.82$, LES_1 (line) *vs.* DNS_1 (circles).

Finally, let us address the subgrid stresses which contribute the term

$$S_3^{sgs} = \frac{2}{4\pi r^2} \oint_{\partial B_r} \langle (\tau_{ik}^{\dagger} + T_{ik}^{\dagger}) \delta \overline{u}_i \rangle n_k \, \mathrm{d}S_r. \tag{4.5}$$

At separations of the order of the filter scale, the energy flux cannot be sustained by the transfer term S_3^{tr} associated with the coarse-grained field, and the subgrid contribution S_3^{sgs} becomes significant. The latter globally represent the scale-energy which is drained from scales larger than r to feed subfilter fluctuations. Its sum with the viscous correction is plotted in figure 8. The agreement with the exact fluxes of the same nature provided by the DNS data is surprising as soon as $L_F < L_S$. The violation of this condition again leads to significant modelling errors.

5. The p.d.f. of the resolved velocity increments and intermittency

So far we have been dealing with low-order observables to show that certain crucial scale-dependent statistical objects, such as the energy transfer, can be reproduced by a suitably designed LES. The target of the present section is a more sophisticated feature of the field, described by the probability distribution function (p.d.f.) of longitudinal velocity increments or, equivalently, by the longitudinal structure functions.

In the homogeneous shear flow, the streamwise velocity increment $\delta u_1(r_1) = u_1(x_1 + r_1, x_2, x_3) - u_1(x_1, x_2, x_3)$ is a random variable whose probability distribution function depends only on separation. The phenomenology of fully developed turbulence implies that, for scales belonging to the classical inertial range, the probability of occurrence of large deviations increases as the separation is progressively reduced. Hence the tails of the p.d.f. decays to zero at a slower rate as the considered scale becomes smaller. This behaviour of the random variable is called intermittent (see e.g. Frisch 1995). Intermittency can be characterized by addressing the scaling laws of the different moments of the p.d.f. – i.e. the structure functions $\langle \delta u_1^p \rangle$ – as functions of the separation. The exponents $\zeta(p)$ of the scaling laws in the inertial range – $\langle \delta u_1^p \rangle \propto r_1^{\zeta(p)}$ – are a convex function of the order of the moment, $(p+1)/3 - p/3 > \zeta(p+1) - \zeta(p)$. As a consequence, the flatness of the p.d.f. – $F_4(r_1) = \langle \delta u_1^4 \rangle / \langle \delta u_1^2 \rangle^2$ – increases as scale separation r_1 is reduced within the inertial range, implying the intermittent behaviour of the signal.

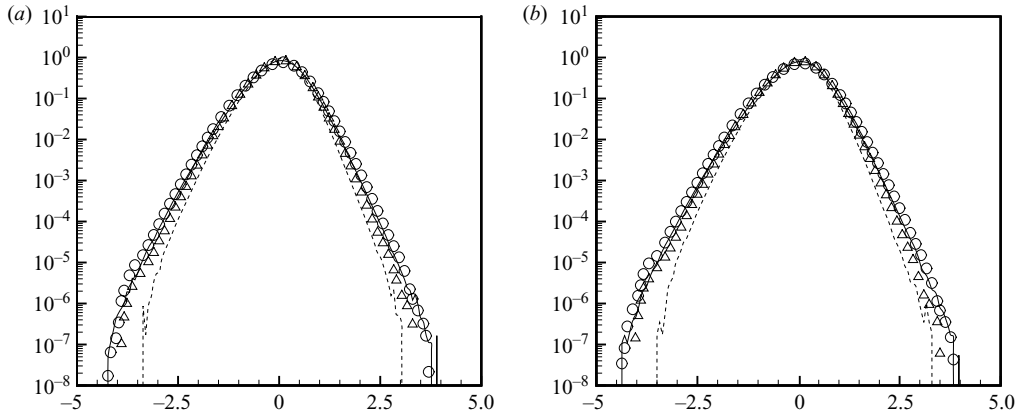

FIGURE 9. Probability density function of the filtered longitudinal velocity increments $\delta\bar{u}_1(r_1) = \bar{u}_1(x_1 + r_1) - \bar{u}_1(x_1)$ at separation (*a*) $r = 29\Delta \simeq 1.42$ and (*b*) $r = 33\Delta \simeq 1.62$. DNS data filtered at $L_F = 0.59$ (circles) and at $L_F = 0.79$ (triangles) and corresponding LES data, solid and dashed line, respectively.

A large-Reynolds-number shear flow is expected to manifest such purely inertial behaviour of the structure functions at small scales, i.e. below L_S. Above the shear scale, the process of turbulent kinetic energy production acts to enhance intermittency (Benzi *et al.* 1999). Clearly, in a number of contexts, intermittency has no practical consequences, and one may be content with LES models able to reproduce accurately only the gross features of the flow. However, there are cases where it is significant, for example, when clustering processes matter, such as for bubbly flows, particle-laden flows, droplets dynamics, spray dynamics or combustion. These large-scale effects belong to the realm of an ideal LES. Whether they are captured by actual LES models is, in fact, an open issue. We attempt to address the subject here by using filtered fields to construct the velocity increments $\delta\bar{u}_1(r_1) = \bar{u}_1(x_1 + r_1, x_2, x_3) - \bar{u}_1(x_1, x_2, x_3)$ and their probability density function, see also Kang *et al.* (2003) for a related discussion on decaying turbulence.

As in previous sections, we contrast LES data with *a posteriori* filtered DNS results. The comparison is presented in figure 9 for the p.d.f. computed at separation $r = 29\Delta \simeq 1.42$ (figure 9*a*) and $r = 33\Delta \simeq 1.62$ (figure 9*b*). Both separations fall in a range of scales above $L_S \simeq 0.72$ and are nominally resolved, i.e. they are larger than the filter scale L_F. Again we discuss two different simulations, with the filter scale, respectively, above and below the shear scale. According to figure 9, the tails of the p.d.f., especially the negative one associated with the energy transfer towards small scale, do not match the filtered DNS when $L_F > L_S$. The agreement is excellent when the shear scale is resolved by the filter. Overall the behaviour is consistent for both separations (figure 9).

From the qualitative analysis of the p.d.f. we anticipate that positioning the filter cutoff below the shear scale is the crucial condition. Once this is accomplished, the LES reproduces the correct intermittency of the field and captures the statistics of the intense fluctuations occurring in the tails of the p.d.f. More quantitative data are provided by the structure functions,

$$\left\langle \delta\bar{u}_1^p(r_1) \right\rangle = \int \xi^p P_{\delta\bar{u}_1}(\xi, r_1)\, \mathrm{d}\xi. \tag{5.1}$$

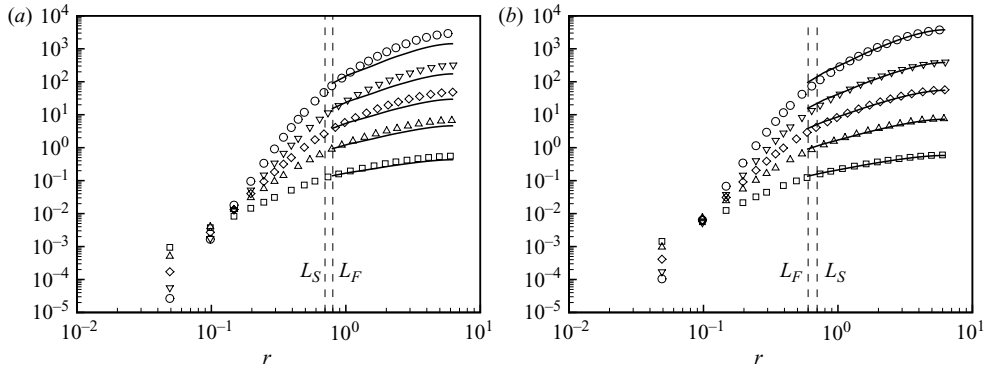

FIGURE 10. Moments of the filtered longitudinal structure functions versus separation. (*a*) LES (lines) and filtered DNS data at $L_F = 0.79$ (symbols). (*b*) LES (lines) and filtered DNS data at $L_F = 0.59$. Symbols correspond to different moments, □, $p = 2$; △, $p = 3$; ◇, $p = 4$; ▽, $p = 5$; ○, $p = 6$. The relative position of the filter scale and the shear scale $L_S = 0.72$ is given by the vertical dashed lines. For easier visualization, $p = 3$ data are multiplied by 10, $p = 4$ by 50, $p = 5$ by 200 and $p = 6$ by a factor 1000.

From the definition, the p.d.f. tails contribute most to the structure functions of high order. Moments up to $p = 6$ are shown in figure 10 for the two LES we have considered. Apparently, when the shear scale is not resolved, the structure functions at scales nominally unaffected by the filter differ more and more from the filtered DNS prediction as p is increased, consistently with the discussed misprediction of the p.d.f. tails. As soon as the shear scale is resolved, the structure functions provided by the LES approach the corresponding filtered DNS data in the whole range of resolved scales. In other words, the condition $L_F < L_S$ must be satisfied to achieve the proper intermittency in shear turbulence.

6. Final remarks

A major issue in turbulence theory concerns the development of subgrid stress models able to achieve a successful simulation of the energy-containing scales of a given flow. However, success is to a large extent a subjective concept related to the goals one has in mind for the simulation. In this paper, we decided to investigate on the conditions under which certain significant features of the large-scale statistics of a turbulent shear flow are reproduced by a specific LES model – in the present case the *ADM*. We stress that no exhaustive investigation of other approaches was attempted, nonetheless the procedure we present can be easily adapted to other subgrid closures.

Different features have been addressed, ranging from single-point objects – e.g. the turbulent shear stress – to a scale energy balance able to assess the performance of the model in capturing the dynamics of the energy-producing scales. We also dealt with higher-order statistics, to understand whether a properly designed LES could reproduce the increase of intermittency which is found in the large scales of shear-dominated flows.

What we have learned was in a sense unexpected. Taking for granted that the low-order statistics may be captured well by a properly designed LES, we expected that the accuracy was bound to deteriorate when dealing with higher-order observables and with the intermittent features of the field. In fact, we discovered that, as soon as the energy-producing scales of the flow are resolved by the LES filter, all the

observables we managed to evaluate were accurately reproduced by the simulation, even the subtle intermittency-increasing effect in high-shear conditions.

Our conclusions are based on the *a posteriori* comparison between LES predictions and DNS data. It is clear that the Reynolds number we used in our tests could not exceed those amenable to DNS, i.e. in the range of small to moderate values. Nonetheless we are confident that our conclusions can be extended to substantially larger values. In fact, experimental data acquired with hot wires in a nominally homogeneous shear flow confirm that the dynamics of the large scales is described well by our LES (Casciola *et al.* 2005).

In the present paper, we have dealt with shear flows away from boundaries. In fact, in a very thin region close to solid walls the matter becomes more complex. Since the shear scale shrinks as the boundary is approached (Pope 2000), our requirement of filter scales smaller than L_S there implies a resolution comparable to a DNS. This is, in fact, a well-established procedure for LES of wall-bounded flows (Baggett *et al.* 1997). Once it is accomplished, our present results predict an almost perfect agreement with filtered DNS even for fine properties of the field such as intermittency. Clearly, in practical applications, the computational demand may become too strong, calling for the use of wall models see e.g. (Cabot & Moin 1999; Piomelli & Balaras 2000). Though extremely important in the industrial context, the adoption of these closures cannot guarantee to match the strict requirements discussed above. Our aim here was to determine the criteria for the preservation of the statistical properties in the LES for shear-dominated conditions. A simulation tool able to address strong shear flows in a range of Reynolds numbers considerably extended with respect to DNS may prove of great value. In fact, it allows us to address, central aspects of the physics of turbulence, such as the failure to recover isotropy at small scales or the shear-induced alteration of the scaling laws thus providing new rational insight for the development of appropriate closures (Casciola *et al.* 2005).

We thank the staff of the compunting center of Rome *CASPUR* where the numerical calculations were done on the IBM System p5 575.

Appendix. Details on the filtering procedure

In this Appendix, we give more details on the explicit filtering procedure. The numerical solution for the homogeneous shear flow is based on the transformation of variables

$$\xi_1 = x_1 - U(x_2)t \quad \xi_2 = x_2 \quad \xi_3 = x_3 \quad \tau = t$$

(Townsend 1956; Rogallo 1981), which maps a fixed box with periodic boundary conditions in computational space into a flow domain in physical space. Given the time-dependence of the transformation, the flow domain becomes distorted like a sheared deck of cards according to the inverse transformation

$$x_1 = \xi_1 + U(\xi_2)\tau \quad x_2 = \xi_2 \quad x_3 = \xi_3 \quad t = \tau.$$

Owing to periodicity in computational space, any field such that

$$\phi(\xi_1, \xi_2, \xi_3) = \phi(\xi_1 + \Lambda_1, \xi_2 + \Lambda_2, \xi_3 + \Lambda_3)$$

is mapped in physical space to a field which features the property

$$\phi(x_1 - U(x_2)t, x_2, x_3) = \phi(x_1 - U(x_2)t + \Lambda_1, x_2 + \Lambda_2, x_3 + \Lambda_3),$$

i.e. it will still be periodic both in x_3 and x_1 for any t, but aperiodic in x_2 unless special conditions are fulfilled. Periodicity in x_2 cannot be achieved for a generic mean profile $U(x_2)$. It occurs, however, for linear mean profiles of the form $U(x_2) = Sx_2$, where it takes place only at time instants that are multiple of the main period $T = \Lambda_1/(S\Lambda_2)$.

The x_1 periodicity can be exploited to obtain the solution in a fixed Cartesian domain in physical space, by shifting the phases of the Fourier transforms in direction 1 by an amount which depends on time and linearly on ξ_2. Starting from the discrete Fourier transform $\hat{\phi}(r_1, r_2, r_3)$ of the field in computational space, where r_1, r_2, r_3 $(-N_{1/2/3} \leqslant r_{1/2/3} \leqslant N_{1/2/3}/2 - 1)$ number the discrete modes in the three directions, the inverse transform gives the field in computational space as

$$\phi(\xi_1, \xi_2, \xi_3, t) = \sum_{r_1, r_2, r_3} \hat{\phi}(r_1, r_2, r_3, t) \exp\left(\jmath \left(\frac{2\pi}{\Lambda_1} r_1 \xi_1 + \frac{2\pi}{\Lambda_2} r_2 \xi_2 + \frac{2\pi}{\Lambda_3} r_3 \xi_3 \right) \right).$$

Introducing Townsend's map we find

$$\phi(x_1, x_2, x_3, t) = \sum_{r_1, r_2, r_3} \hat{\phi}(r_1, r_2, r_3, t) \exp\left(-\jmath \frac{2\pi}{\Lambda_1} r_1 S x_2 t \exp\left(\jmath \left(\frac{2\pi}{\Lambda_1} r_1 x_1 + \frac{2\pi}{\Lambda_2} r_2 x_2 + \frac{2\pi}{\Lambda_3} r_3 x_3 \right) \right) \right),$$

an expression that can be used for the evaluation in physical space. In particular, it allows us to reconstruct the field ϕ at any time in a fixed reference Cartesian box. All we need is the phase shift of the computational-space discrete transforms,

$$\hat{\phi}_s(r_1, r_2, r_3, t) = \hat{\phi}(r_1, r_2, r_3, t) \exp\left(-\jmath \frac{2\pi}{\Lambda_1} r_1 S \Delta_2 r_2 t \right),$$

where Δ_2 is the grid spacing in direction 2. This simple rule is able to generate by inverse Fourier transform the field in the unskewed reference grid. By introducing the nodal indices of the Cartesian grid – $x_1 = l_1 \Delta_1$, $x_2 = l_2 \Delta_2$, $x_3 = l_3 \Delta_3$, $(l_{1/2/3} = 1, \ldots, N_{1/2/3})$ – the discrete field reads

$$\phi(l_1, l_2, l_3, l) = \sum_{r_1, r_2, r_3} \hat{\phi}_s(r_1, r_2, r_3, t) \exp\left(\jmath \left(\frac{2\pi}{N_1} r_1 l_1 + \frac{2\pi}{N_2} r_2 l_2 + \frac{2\pi}{N_3} r_3 l_3 \right) \right).$$

We will address the above phase shifting as a re-meshing procedure applied in Fourier space. As it is clear from the definition, the final field will be aperiodic in x_2 (see e.g. ((Gualtieri *et al.* 2002) and references therein for more details).

After having recalled a few preliminary technicalities, let us move to the crucial issue of filtering. In physical space, the LES filter kernel $G(x_1, x_2, x_3 | x_1', x_2', x_3')$ has compact support. It is built as the Cartesian product of one-dimensional filters invariant under translations – i.e. $G = g(x_1 - x_1') g(x_2 - x_2') g(x_3 - x_3')$ – with cutoff length scale L_F identical in all three directions and uniform in space. The simplest way to apply filtering is to operate on the Cartesian grid. The coarse-grained field $\overline{\phi}$ is obtained by convolution of the filter G with the fine-grained field ϕ,

$$\overline{\phi}(x_1, x_2, x_3) = \int G(x_1 - x_1', x_2 - x_2', x_3 - x_3') \, \phi(x_1', x_2', x_3') \, \mathrm{d}x_1' \, \mathrm{d}x_2' \, \mathrm{d}x_3'.$$

In numerics we deal with discrete signals, so that the discrete filter becomes $G = g(l_1 - l_1')g(l_2 - l_2')g(l_3 - l_3')$ and convolution sums replace convolution integrals,

$$\overline{\phi}(l_1, l_2, l_3) = \sum_{l_1', l_2', l_3'} g(l_1 - l_1')g(l_2 - l_2')g(l_3 - l_3')\,\phi(l_1', l_2', l_3')$$
$$= \sum_{l_1'', l_2'', l_3''} g(l_1'')g(l_2'')g(l_3'')\,\phi(l_1 + l_1'', l_2 + l_2'', l_3 + l_3'').$$

As already stated, the discrete field is periodic in directions 1 and 3. The convolution theorem allows us less to replace the l_1'' and l_3'' sums by products of the discrete Fourier transforms followed by a Fourier inverse transformation. Concerning direction 2, the lack of periodicity forces us to work in physical space. In fact, at each time step, by using the re-meshing procedure, the velocity field in the physical unskewed grid is reconstructed and the filter is applied in the direction of the mean velocity gradient with explicit use of the respective convolution sum. Finally, the filtered field is mapped back into computational space.

The filters used in our simulations have been built according to Vasilyev, Lund & Moin (1998), where all the details may be found. Here we simply give the technical specifications which identify our filters. The general prescription calls for the following properties of the one-dimensional filter kernel g in terms of its Fourier transform expressed as a function of the dimensionless wavenumber $\omega = k\Delta$, with Δ the grid spacing: $\hat{g}(0) = 1$, $\hat{g}(\pi) = 0$, $M^k g = 0 \quad k = 1, \ldots, 3$, ($M^k$ denote the kth moment of the filter), $\mathrm{d}\hat{g}/\mathrm{d}\omega|_\pi = 0$ and the dimensionless cutoff wavenumber ω_F is imposed by $|\hat{g}(\omega_F)| = 1/2$. In directions 1 and 3, with the same grid spacing $\Delta_1 = \Delta_3$, $\omega_F = 2\pi/3$ and the filter is the same. Given the different grid spacing $\Delta_2 = \Delta_{1/3}/2$, in direction 2 we have selected $\omega_F = \pi/3$, in order to have the same cutoff length-scale $L_F = 2\pi/k_F = 2\pi\Delta/\omega_F$ in all three spatial directions.

REFERENCES

Antonia, R. A., Djenidi, L. & Spalart, P. R. 1994 Anisotropy of the dissipation tensor in a turbulent boundary layer. *Phys. Fluids* **6**(7), 2475–2479.

Baggett, J. S., Jimenez, J. & Kravshenko, A. K. 1997 Resolution requirements in large-eddy simulation of shear flows. *CTR Annu. Res. Briefs.*

Benzi, R., Amati, G., Casciola, C. M., Toschi, F. & Piva, R. 1999 Intermittency and scaling laws for wall bounded turbulence. *Phys. Fluids* **11**, 1284.

Biferale, L. & Procaccia, I. 2005 Anisotropy in turbulent flows and in turbulent transport. *Phys. Rep.* **414**(2–3), 1–150.

Cabot, W. & Moin, P. 1999 Aproximate wall boudary conditions in the large eddy simulation of high Reynolds number. *Flow Turbulence. Combust.* **63**, 269–291.

Carati, D., Winckelmans, G. S. & Jeanmart, H. 2001 On the modelling of the sub-grid scale and filtered-scale stress tensors in large-eddy simulation. *J. Fluid Mech.* **441**, 119–138.

Casciola, C. M., Gualtieri, P., Benzi, R. & Piva, R. 2003 Scale by scale budget and similarity laws for shear turbulence. *J. Fluid Mech.* **476**, 105–114.

Casciola, C. M., Gualtieri, P., Jacob, B. & Piva, R. 2005 Scaling properties in the production range of shear dominated flows. *Phys. Rev. Lett.* **95**, 225–245.

Cerruti, S. & Meneveau, C. 2000 Statistics of filtered velocity in grid and wake turbulence. *Phys. Fluids* **12**(5), 1143–1165.

Champagne, F. H., Harris, V. G. & Corrsin, S. 1970 Experiments on nearly homogeneous turbulent shear flow. *J. Fluid Mech.* **41**, 81–139.

Chow, F. K. & Moin, P. 2003 A further study of numerical errors in large-eddy simulatios. *J. Comput. Phys.* **184**, 366–380.

Corrsin, S. 1958 On local isotropy in turbulent shear flow. *NACA R & M* **58B11**.

Domaradsky, J. A. & Loh, K. C. 1999 The subgrid-scale estimation model in the physical space representation. *Phys. Fluids* **11**(8), 2330–2342.

Domaradsky, J. A. & Saiki, E. M. 1997 A subgrid-scale model based on the estimation of unresolved scales of turbulence. *Phys. Fluids* **9**(7), 2148–2164.

Durbin, P. A. & Speziale, C. G. 1997 Local anisotropy in strained turbulence at high Reynolds number. *Trans. ASME* I: *J. Fluid Engng* **113**, 707–709.

Ferchichi, M. & Tavoularis, S. 2000 Reynolds number effects on the fine structure of uniformly shared turbulence. *Phys. Fluids* **12**(11), 2942–2953.

Freitag, M. & Klein, M. 2006 An improved method to assess the quality of large eddy simulation in the context of implicit filtering. *J. Turbulence* **7**(40), 1–12.

Frisch, U. 1995 *Turbulence*. Cambridge University Press.

Garg, S. & Warhaft, Z. 1998 On the small scale structures of simple shear flow. *Phys. Fluids* **10**(3), 662–673.

Ghosal, S. 1996 An analysis of numerical error in large-eddy simulations of turbulence. *J. Comput. Phys.* **125**, 187–206.

Gualtieri, P., Casciola, C. M., Benzi, R., Amati, G. & Piva, R. 2002 Scaling laws and intermittency in homogeneous shear flow. *Phys. Fluids* **14**(2), 583–596.

Guerts, B. J. 1997 Inverse modeling for large-eddy simulation. *Phys. Fluids* **9**(12), 3585–3588.

Guerts, B. J. & Frohlich, J. 2002 A framework for predicting accuracy limitations in large-eddy simulation. *Phys. Fluids* **14**(6), L41–L44.

Guerts, B. J. & Holm, D. D. 2003 Regularization modeling for large-eddy simulation. *Phys. Fluids* **15**(1), L13–L16.

Gullibrand, J. & Chow, F. K. 2003 The effect of numerical errors and turbulence models in large-eddy simulations of channel flow, with and without explicit filtering. *J. Fluid Mech.* **495**, 323–341.

Harris, V. G., Graham, J. A. H. & Corrsin, S. 1977 Further experiments in nearly homogeneous turbulent shear flow. *J. Fluid Mech.* **81**, 657–687.

Jacob, B., Biferale, L., Iuso, G. & Casciola, C. M. 2004 Anisotropic fluctuations in turbulent shear flows. *Phys. Fluids* **16**(11), 4135–4142.

Jimenez, J. & Moser, R. D. 2000 Large-eddy simulation: where are we and what can we expect? *AIAA J.* **4**, 605–612.

Kang, H. S., Chester, S. & Meneveau, C. 2003 Decaying turbulence in active-grid-generated flow and comparison with large-eddy simulation. *J. Fluid Mech.* **480**, 129–160.

Kida, S. & Tanaka, M. 1994 Dynamics of vortical structures in homogeneous shear flow. *J. Fluid Mech.* **274**, 43–68.

Klein, M. 2005 An attempt to assess the quality of large eddy simulation in the context of implicit filtering. *Flow Turbulence Combust.* **75**, 133–166.

Kolmogorov, A. N. 1941 The local structure of turbulence in incompressible viscous fluid for very large Reynolds number. *Dokl. Akad. SSSR* **434**.

Kurien, S. & Sreenivasan, K. R. 2002 Anisotropic scaling contributions to high-order structure functions in high-Reynolds-number turbulence. *Phys. Rev.* E **62**(2), 2206–2212.

Langford, J. A. & Moser, R. D. 1999 Optimal LES formulations for isotropic turbulence. *J. Fluid Mech.* **398**, 321–346.

Lee, M. J., Kim, J. & Moin, P. 1990 Structure of turbulence at high shear rate. *J. Fluid Mech.* **216**, 561–583.

Lesieur, M. & Metais, O. 1996 New trends in large eddy simulation of turbulence. *Annu. Rev. Fluid Mech.* **28**, 45–82.

Lilly, D. K. 1967 The representation of small scale turbulence in numerical simulation experiments. *Proc. IBM Scientific Computing Symp. Environ. Sci.*

Marati, N., Casciola, C. M. & Piva, R. 2004 Energy cascade and spatial fluxes in wall turbulence. *J. Fluid Mech.* **521**, 191–215.

Mathew, J., Lechner, R., Foysi, H., Sesterhenn, J. & Friedrich, R. 2003 An explicit filtering method for large eddy simulation of compressible flows. *Phys. Fluids* **15**(8), 2279–2289.

Mathew, J., Foysi, H. & Friedrich, R. 2006 A new approach to LES based on explicit filtering. *Intl J. Heat Fluid Flow* **27**, 595–602.

Meneveau, C. 1994 Statistics of turbulence subgrid-scales stresses: necessary conditions and experimental tests. *Phys. Fluids* **6**(2), 815–833.

Meneveau, C. & Katz, J. 2000 Scale-invariance and turbulence models for large eddy simulation. *Annu. Rev. Fluid Mech.* **32**, 1–32.

Meyers, J., Guerts, B. J. & Baelmans, M. 2003 Database analysis of errors in large-eddy simulation. *Phys. Fluids* **15**(6), 2740–2755.

Moin, P. 2002 Advances in large eddy simulation methodology for complex flows. *Intl J. Heat Fluid Flow* **23**, 710–720.

Moin, P. & Apte, S. V. 2006 Large-eddy simulation of realistic gas turbine combustors. *AIAA J.* **44**(4), 698–708.

Piomelli, U. & Balaras, E. 2000 Wall-layer models for large-eddy simulations. *Annu. Rev. Fluid Mech.* **34**, 349–374.

Piomelli, U., Moin, P. & Ferziger, J. H. 1988 Model consistency in large eddy simulation of turbulent channel flow. *Phys. Fluids* **31**(7), 1884–1891.

Pope, S. B. 2000 *Turbulent Flows*. Cambridge University Press.

Pope, S. B. 2004 Ten questions concerning the large eddy simulation of turbulent flows. *New J. Phys.* **6**, 1–24.

Pumir, A. 1996 Turbulence in homogeneous shear flow. *Phys. Fluids* **8**(11), 3112–3127.

Pumir, A. & Shraiman, B. 1994 Persistent small scale anisotropy in homogeneous shear flow. *Phys. Rev. Lett.* **75**(11), 3114–3117.

Rogallo, R. S. 1981 Numerical experiments in homogeneous turbulence. NASA TM 81315.

Rogers, M. M. & Moin, P. 1987 The structure of the vorticity field in homogeneous turbulent flows. *J. Fluid Mech.* **176**, 33–66.

Rohr, J. J., Itsweire, E. C., Helland, K. N. & Van Atta, C. W. 1988 An investigation of the growth of turbulence in a uniform-mean-shear flow. *J. Fluid Mech.* **187**, 1–33.

Rose, W. G. 1966 Results of an attempt to generate a homogeneous turbulent shear flow. *J. Fluid Mech.* **25**, 97–120.

Saddoughi, S. G. & Veeravalli, S. V. 1994 Local isotropy in turbulent boundary layer at high Reynolds number. *J. Fluid Mech.* **268**, 333–372.

Shen, X. & Warhaft, Z. 2000 The anisotropy of small scale structures in High Reynolds number ($Re_\lambda \sim 1000$) turbulent shear flow. *Phys. Fluids* **12**(11), 2976–2989.

Shumacher, J. 2001 Derivative moments in stationary homogeneous shear turbulence. *J. Fluid Mech.* **441**, 109–118.

Shumacher, J. 2004 Relation between shear parameter and Reynolds number in statistically stationary turbulent shear flows. *Phys. Fluids* **16**(8), 3094–3102.

Shumacher, J. & Eckhardt, B. 2000 On statistically stationary homogeneous shear turbulence. *Europhys. Lett.* **52**, 627–632.

Shumacher, J., Sreenivasan, K. R. & Yeung, P. K. 2003 Derivative moments in turbulent shear flows. *Phys. Fluids* **15**(1), 84–90.

Smagorinsky, J. 1963 General circulation experiments with the primitive equations. I. The basic experiments. *Mon. Weather Rev.* **91**.

de Souza, F. A., Nguyen, V. D. & Tavoularis, S. 1995 The structure of highly sheared turbulence. *J. Fluid Mech.* **303**, 155–167.

Spalart, P. R. 1988 Direct simulation of a turbulent boundary layer uo to $Re_\theta = 1410$. *J. Fluid Mech.* **187**, 61–98.

Stolz, S. & Adams, N. A. 1999 An approximate deconvolution procedure for large-eddy simulation. *Phys. Fluids* **11**(7), 1699–1701.

Stolz, S., Adams, N. A. & Kleiser, L. 2001 An approximate deconvolution procedure for large-eddy simulationi with application to incompressible wall-boubnded flows. *Phys. Fluids* **13**(4), 997–1015.

Tavoularis, S. & Corrsin, S. 1981*a* Experiments in nearly homogeneous turbulent shear flow with a uniform mean temperature gradient. Part 1. *J. Fluid Mech.* **104**, 311–347.

Tavoularis, S. & Corrsin, S. 1981*b* Experiments in nearly homogeneous turbulent shear flow with a uniform mean temperature gradient. Part 2. The fine structure. *J. Fluid Mech.* **104**, 349–367.

Tavoularis, S. & Karnik, U. 1989 Further experiments on the evolution of turbulent stresses and scales in uniformly sheared turbulence. *J. Fluid Mech.* **204**, 457–478.

Townsend, A. A. 1956 *The Structure of Turbulent Shear Flow*. Cambridge University Press.

Vasilyev, O., Lund, T. S. & Moin, P. 1998 A general class of commutative filters for LES in complex geometries. *J. Comput. Phys.* **146**, 82–104.

Warhaft, Z. & Shen, X. 2002 On higher order mixed structure functions in laboratory shear flow. *Phys. Fluids* **14**(7), 2432–2438.

Winckelmans, G. S., Wray, A. A. & Jeanmart, H. 2001 Explicit-filtering large-eddy simulation using the tensor-diffusivity model supplemented by a dynamic Smagorinsky term. *Phys. Fluids* **13**(5), 1385–1403.

Yakhot, V. 2003 A simple model for self-sustained oscillations in homogeneous shear flow. *Phys. Fluids* **15**(2), L17–L20.